Dissimilar friction stir welding of AA2198 and AA7475: Effect of solution treatment and aging on the microstructure and mechanical strength

Dissimilar friction stir welding of AA2198 and AA7475: effect of solution treatment and aging on the microstructure and mechanical strength

M.R. Jandaghi *, C. Badini, M. Pavese

Department of Applied Science and Technology, Politecnico di Torino, Corso Duca degli Abruzzi 24, 10129 Torino, Italy

**Corresponding author; E-mail: mohammadreza.jandaghi@polito.it*

Abstract

A post-weld heat treatment consisting of solution treatment and subsequent aging (STA) is widely applied to aluminum joints fabricated by friction stir welding (FSW) to improve the mechanical strength via precipitation hardening. In this study, aerospace aluminum alloys of AA2198 and AA7475 were FSWed in similar and dissimilar states. Differential scanning calorimetry (DSC) was used to trace the precipitation strengthening during the aging of welded specimens. The post-weld aging procedures were designed based on the DSC outputs. Accordingly, welded sheets were solution treated at 480 °C and 540 °C for 10 to 90 min, air-cooled and aged at 155 °C and 170 °C for 2 to 40 h, respectively. Optical micrographs revealed that due to the faster kinetics of the recrystallization, higher homogenizing temperature led to nucleation of the finer grains from highly stress localized points in the stir zone (SZ) and TMAZ by faster growth rate. Higher time and temperature of the solution-treatment eventuated in accumulation of Cu-enriched intermetallic phases in the grain boundaries at SZ and TMAZ of AA7475, attenuation of the grains adhesion and failure of the sample. Hardness test results showed that the hardness increased in AA7475 alloy while decreasing in AA2198 alloy in the as-welded state. Post weld heat treatment enhanced the hardness in AA2198 and reduced it in AA7475. However, it had no significant effect on the grain size.

Keywords: *Friction Stir Welding; Aluminum Alloy; Dissimilar Welding; Microstructure; Hardness.*

Introduction

In recent decades, friction stir welding (FSW) as a method for solid-state welding of the aluminum alloys has come to the spotlight of the welding engineers and exploited in many industrial applications [1-3]. The low weight/volume ratio of the aluminum alloys beside notable susceptibility to a broad range of phase transformations has made them interesting for welding development through different methods such as FSW [4-11]. Nevertheless, stir welding does not confine to bonding the aluminum alloys and was extensively utilized for other metals like copper

[12-14], titanium [15], magnesium [16], steels [17-20], Pb [21] and Ni alloys [22]. During the FSW process, a non-consumable rotating pin moves between the metallic plates, and because of the heat accumulation under the pin, intense turbulence creates between the semi-solid materials and welds the sheets [2]. Delijaicov et al. pointed to the rotational speed and proceeding rate as the most determinative parameters in the FSW process that control the heat input and flow of the material [23]. Formerly, FSW was repeatedly examined on the aluminum alloys, which have weak weldability, namely as 7xxx and 2xxx series as similar [24-26] and dissimilar [27-29] modes. Among these materials, Al-Cu-Li (AA2198) and Al-Zn-Mg (AA7475) are of the third-generation advanced aluminum alloys largely used in aerospace applications. The attendance of Li in Al-Cu-Li alloy not only can lessen the density but also can enhance the elastic modulus and specific strength [30]. In a most recent application, AA2198 is employed in the skin of two-stage rocket SpaceX Falcon9 [31]. Based on the literature, during the FSW of AA2198, an increase in the rotational speed can displace the failure point from HAZ to the TMAZ/SZ border [32]. Goebel et al. argued that the HAZ and frontier of TMAZ/SZ are more vulnerable points for failure. The weakness of HAZ arises from partial precipitation owing to thermal cycles, while the SZ/TMAZ interface suffers from a lack of strong bonding due to residual stress [31]. Milagre et al. studied the phase transformation in similar FSWed AA2198 alloys. They claimed that the key phases at the base metal were T1 (Al_2CuLi) θ' (Al_2Cu), δ'/β'(Al_3(Li,Zr)) and Ω (Al_2Cu). Based on their observation, regardless of retreating or advancing side, HAZ was free of the θ' phase. In the TMAZ, T1, δ'/β', GP zones phase were observed in the retreating side, while T1 and GP zones were detected. Also in the SZ, GP zones, T1, δ'/β' (Al_3(Li,Zr)) and Ω were traced [33]. Entringer et al. explored the effect of the Cu/Li ratio on the precipitation. They declared that a low Cu/Li ratio induced softer behavior and reduced the yield strength of the base metal. However, the high Cu/Li ratio improved the thermal stability, dissolution of the T1 phase, formation of equilibrium phases in SZ, and homogenizing and overaging in HAZ [34]. Stir welding of AA7475 has also studied previously. Reddy et al. [35] investigated the FSW of AA7475-T761 sheets and argued that the welding center includes the finest microstructure displayed the maximum hardness value. Furthermore, their observations indicated that $MgZn_2$, Al_2Cu, and Al_2CuMg were the main particles often formed in SZ of AA7475. Kalashnikova et al. announced that during similar welding of AA7475, stir zone have the finest grains by the most uniform distribution of the particles [36]. Jacob et al. stated that during FSW of AA7475, choosing a high rotational speed (1120 rpm), a very low proceeding rate (63 mm/min), and cooling through the ice slush could suppress the precipitate coarsening and encourage the ultrafine graining [37]. However, Gupta et al. [38] and Goel et al. [39] recommended the 400 and 560 rpm as the best rotational speed for similar welding of AA7475, respectively. It has proved that in similar welding of AA7475, defects were mostly formed in the TMAZ and HAZ and led to hardness attenuation [40]. A similar observation

was also described by Zaman Khan et al. on the joining of AA2219 to AA7475 [41]. To improve the weldability and mechanical strength of the AA2XXX and AA7XXX joints, some researchers added a little of powders like B_4C and CeO_2 to the aluminum matrix before FSW [42]. Nevertheless, STA is the most common way to improve the strength and formability of the FSWed sheets up to the desired level [43-46]. The aged samples often will overage during FSW from HAZ and parts of the TMAZ. Essentially STA could increase the hardness due to precipitation hardening [47]. To assess the effect of aging on properties of the fabricated joint between aluminum alloys, often FSWed sheets undergone solution-treatment at a temperature range of 460-580 °C for 0.5-4 h [48-51]. As a result, often most of the precipitates dissolve in the matrix, and final quenching prevents from nucleation of the new particles. In the following, supplementary aging at a temperature range of 120-190 °C for 1-30 h exerts to the samples [52-55]. Consequently, gradual germination of fine particles leads to precipitate hardening and enhancement of mechanical strength.

In the current research, the influence of STA on mechanical properties and microstructural evolutions of FSWed AA2198-T3 and AA7475-W as similar and dissimilar was investigated. Microstructural observations were authorized by XRD and DSC outputs to explore the phase transformations. Eventually, mechanical behavior was validated by microstructural evidence and failure analysis, and the most efficient STA procedure was introduced.

Experimental procedure

Aluminum sheets of AA2198-T3 and 7475-W with an initial thickness of 3 mm were supplied by Alenia Aeronautica aerospace company. Chemical composition of examined alloys is presented in Fig. 1.

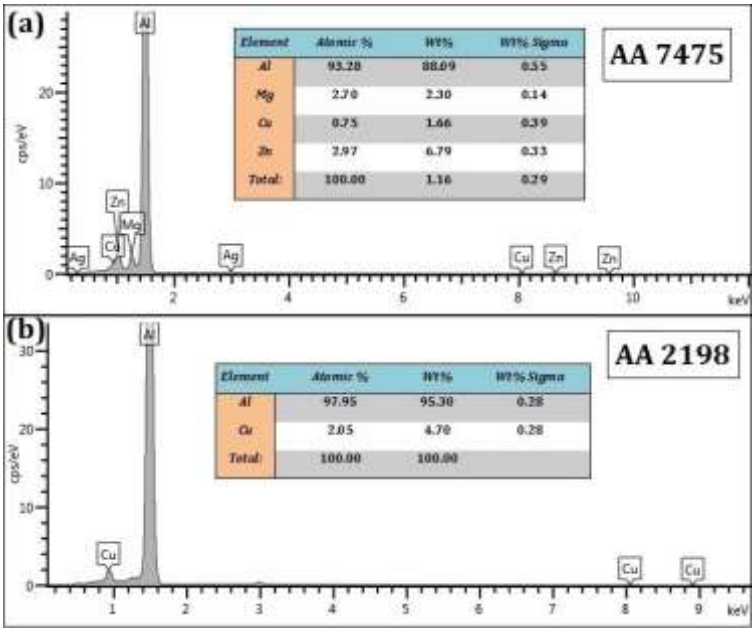

Fig. 1: Chemical composition of employed 2198 and 7475 aluminum alloys revealed by EDS.

The small atomic weight of Li hindered its recognition through the EDS detector. However, XRD analysis unveiled it in the AA2198 structure. As can be seen, Zn and Mg were the main alloying elements in AA7475, while Cu was the dominant alloying element in AA2198. FSW performed in both similar and dissimilar states by employing a tool having a 13.45 mm shoulder diameter and a pin with a 4.7 mm diameter and 3.16 mm height. The progress angle, traverse, and rotational speeds of the tool considered as 2°, 50 mm/min, and 830 rpm, respectively. Welding tool assembled on a milling machine. Schematic representation of the welding process and practical image of dissimilarly welded alloys have been displayed in Fig. 2.

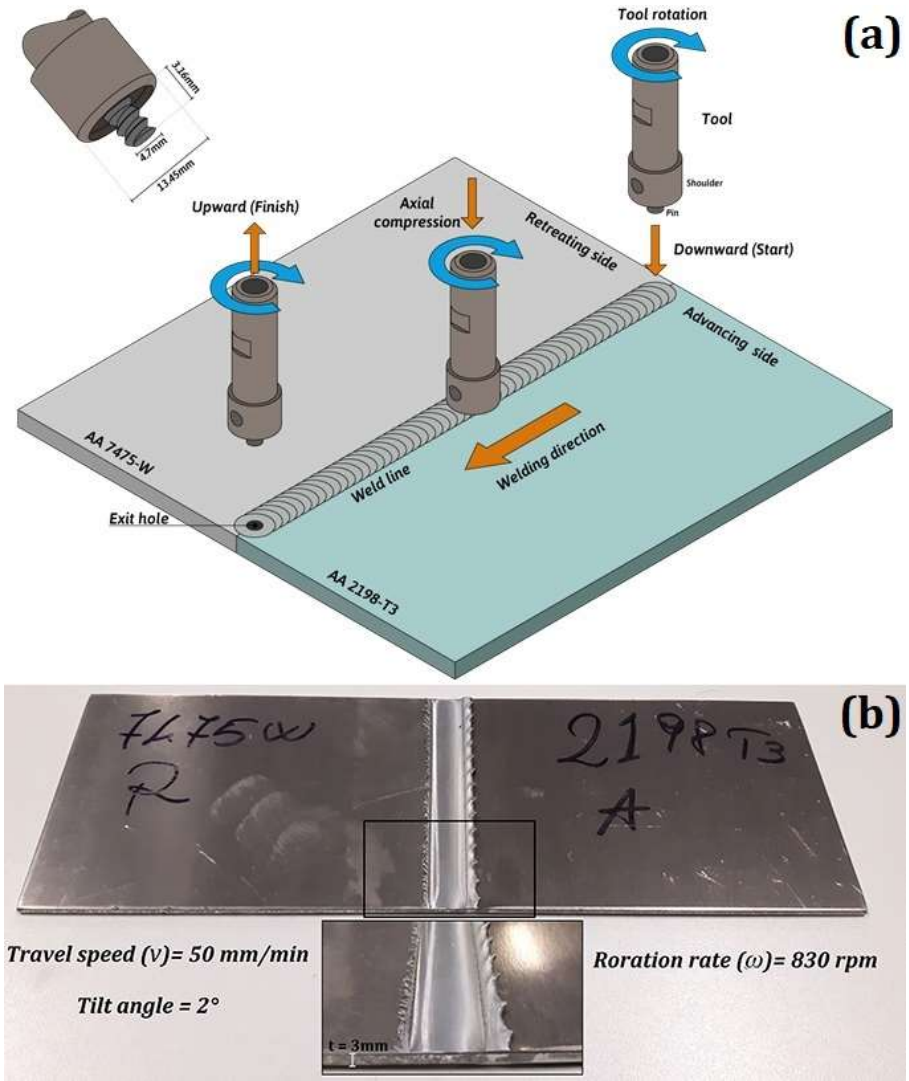

Fig. 2: Schematic representation of the FSW process (a) and dissimilar welding between AA7475-W and AA2198-T3 (b).

Hardness variation was measured along the cross-section of the welded sheets using the Brinell tool equipped to an indenter with 2.5 mm diameter imposing load of 50 kg. For metallographic observations, the cross-section of the welded specimens was mechanically polished by SiC papers and diamond suspension and etched using Keller and barker reagents. Variation of chemical

composition in weld constituents and precipitates was tracked by scanning electron microscope (SEM) equipped to an energy dispersion spectroscopy (EDS) detector. X-ray analysis aided to validate the SEM results. For checking the phase transition temperatures, small parts of the weld line were analyzed by differential scanning calorimetry (DSC) under a dynamic argon atmosphere, scanning rate 20°C/min. DSC samples were annealed at 550 °C for 4 h under argon atmosphere and quenched in the water. All the welded specimens have been aged in an oil bath with constant temperature in two steps; short-term aging at 120 °C for 3 h and subsequent long-term aging at 155 °C and 170 °C. Microstructure and mechanical strength in different specimens before and after STA were evaluated using OM and Brinell hardness, respectively.

Results and discussion

Microstructure variation in cross-section of the weld line is presented in Fig. 3.

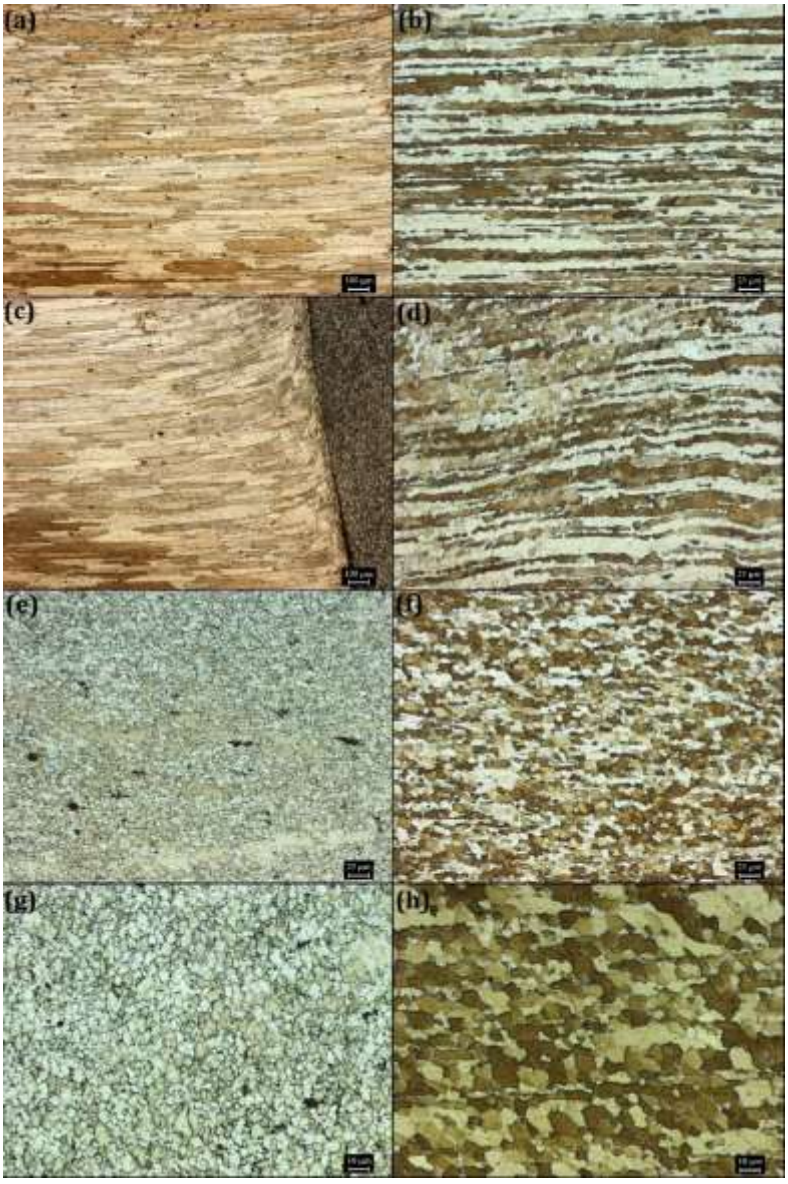

Fig. 3: Variation of size and morphology of grains in AA7475 and AA2198 after dissimilar welding in base metal (a, b), HAZ to SZ (c, d), SZ (e, f) and higher magnification of SZ (g, h), respectively.

Comparison of Fig. 3(a) and 3(b), indicated that the grains were elongated in base metals. The morphology of grains in HAZ and TMAZ of the dissimilar joint has been demonstrated in Figs. 3(c) and 3(d). The noticeable difference between AA7475 and AA2198 was the sharp refinement of grains at the SZ border of AA7475 (Fig. 3c). However, in AA2198 side, grains refined gradually along with partial recrystallization from HAZ to SZ. Figs. 3(e) and 3(f) show the grain size distribution inside the SZ of AA7475 and AA2198, respectively. On both sides, grains had the same morphology and non-uniform distribution. In-depth analysis in higher magnifications (Figs. 3g and 3f) worthy proved that semi-equiaxed grains in SZ of AA7475 were finer than AA2198 counterpart.

The microstructure of different regions formed by the rotary shoulder is depicted in Fig. 4.

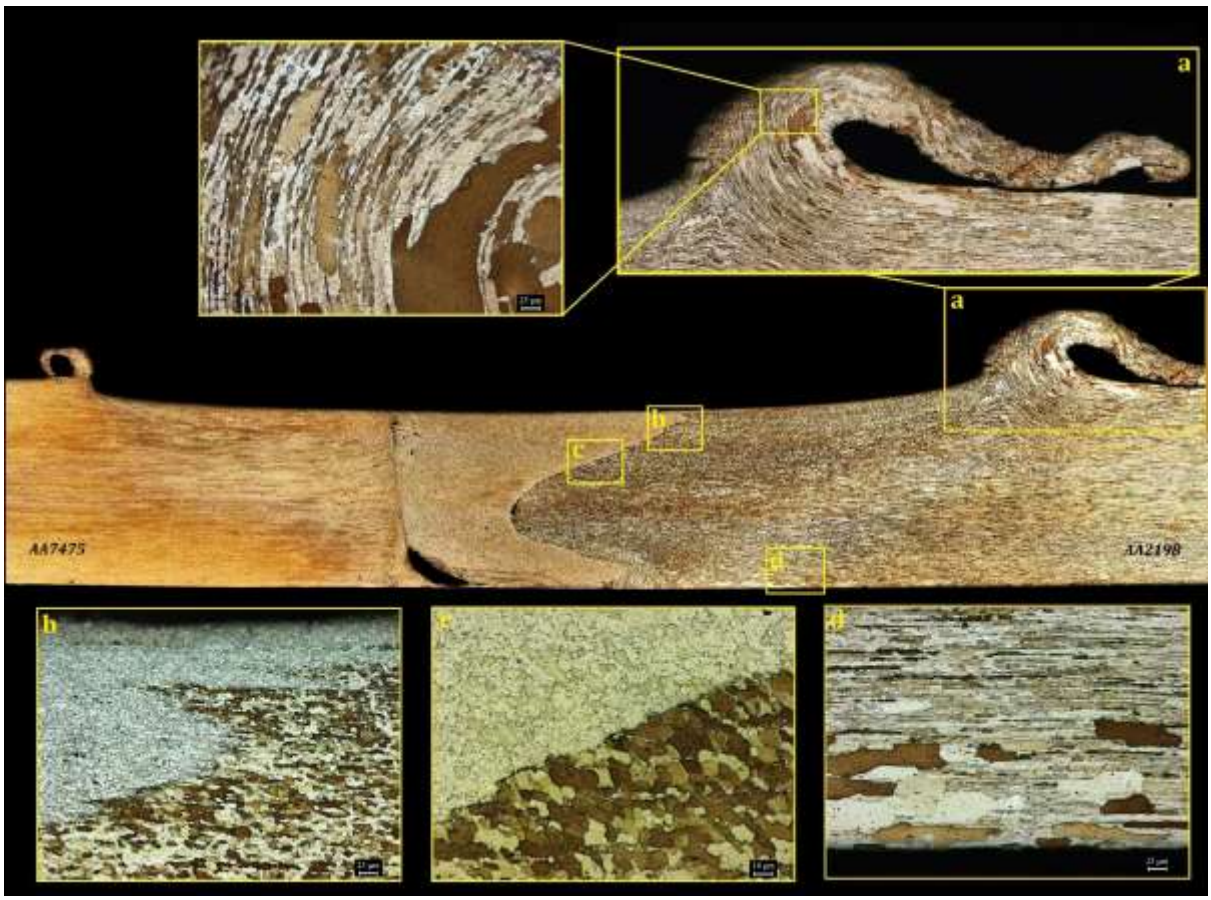

Fig. 4: Microstructure of (a) welding edge, (b) grain refinement close to the surface in SZ, (c) grain size variation at the interface of AA7475 and AA2198, and (d) coarse grains in HAZ of AA2198.

The welding margin that was in direct touch with a rotating pin contains a grain gradient (Fig. 4a). The layers closer to the shoulder had finder grains. According to Fig. 4(b), areas under the shoulder and near the surface have the finest grains. Furthermore, the grains of AA2198 and AA7475 had not the same size in SZ and were distinct from each other by a sharp interface (Fig. 4c). A similar observation is also reported on FSWed AA2219-O to AA7475-T761 [56]. Accordingly, partial recrystallization and precipitate strengthening starts from the TMAZ and

continues up to HAZ. Detailed structural analysis indicated that the bottom of AA2198 under the shoulder involves some coarse grains. Grain coarsening there could be attributed to insufficient heat dissipation under the pin. The creation of a small hole under the pin is known as a tunneling defect, which usually arises from a low tilt angle of the shoulder. To avoid the tunneling fault, it is crucial to perform the welding at high enough temperatures. As a result, it is necessary to work at a high rotational speed and low progress speed [23]. To explore the lattice parameters and second phase particles in the dissimilar joint, XRD patterns were analyzed (Fig. 5).

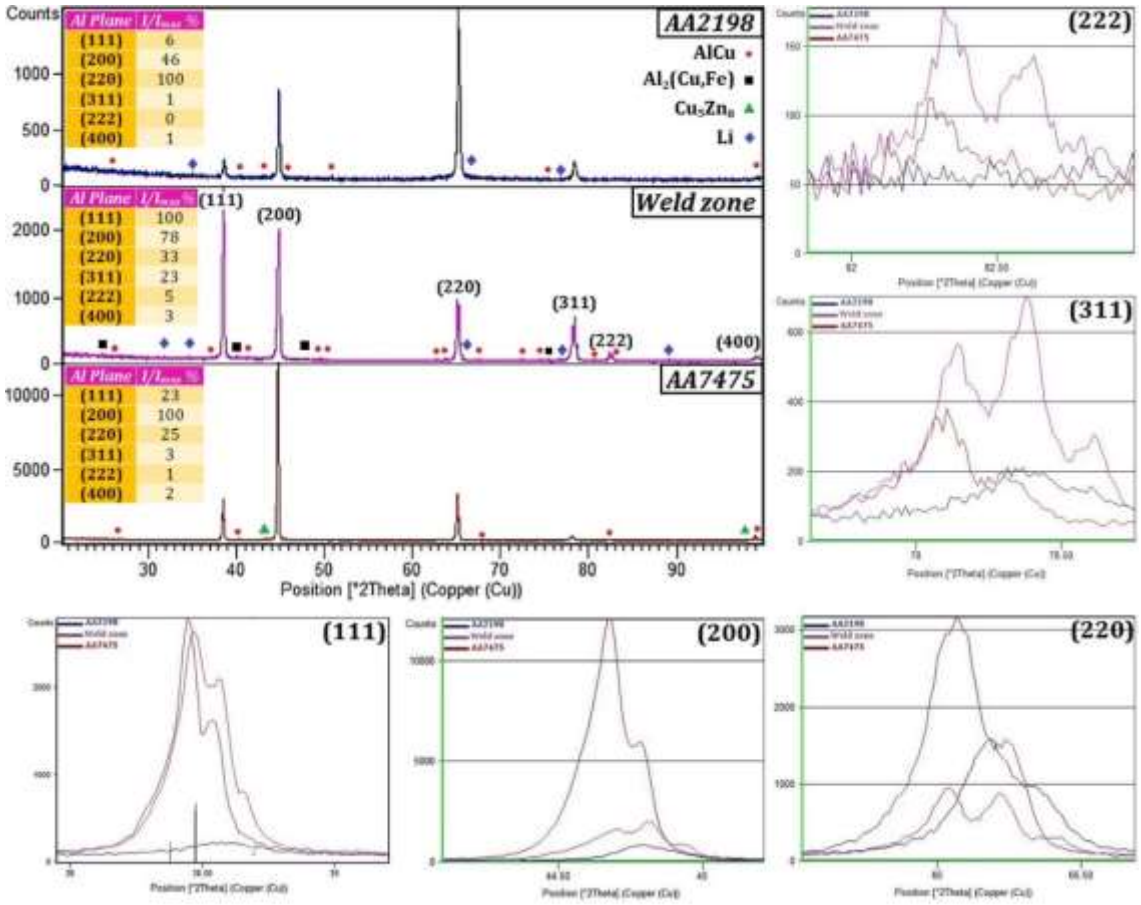

Fig. 5: XRD pattern of different zones in the as-weld specimen.

According to the literature, the main strengthening phases in AA2198 alloy aged at 155°C were Al_2CuLi (T1) [57], Al_3Li (δ') and Al_2Cu (θ'). In SZ, the dissolution of the T1 phase results in δ' and θ' formation [58, 59]. However, the analysis of XRD patterns did not show the peak of Li-contain compounds here. It can be attributed to two main origins. Firstly, in low amounts of Li (0.8-1.1% Li), the formation of Al-Li compounds is more probable in elevated temperatures. So maybe Li compounds were negligible or could not form during the process. Also, considering that the δ' phase has FCC structure, the principal atomic planes of the Al and δ' phase were in the same positions and it was not detected [60-63]. $Al_2(Cu,Fe)$ and AlCu were the main particles precipitated in the SZ. Evaluation of the lattice parameters by XRD showed that in the (111) plane

had the maximum peak intensity ratio in SZ. In order to authorize the XRD outputs, the chemical composition of particles in base metals and SZ measured by the EDS (Fig. 6).

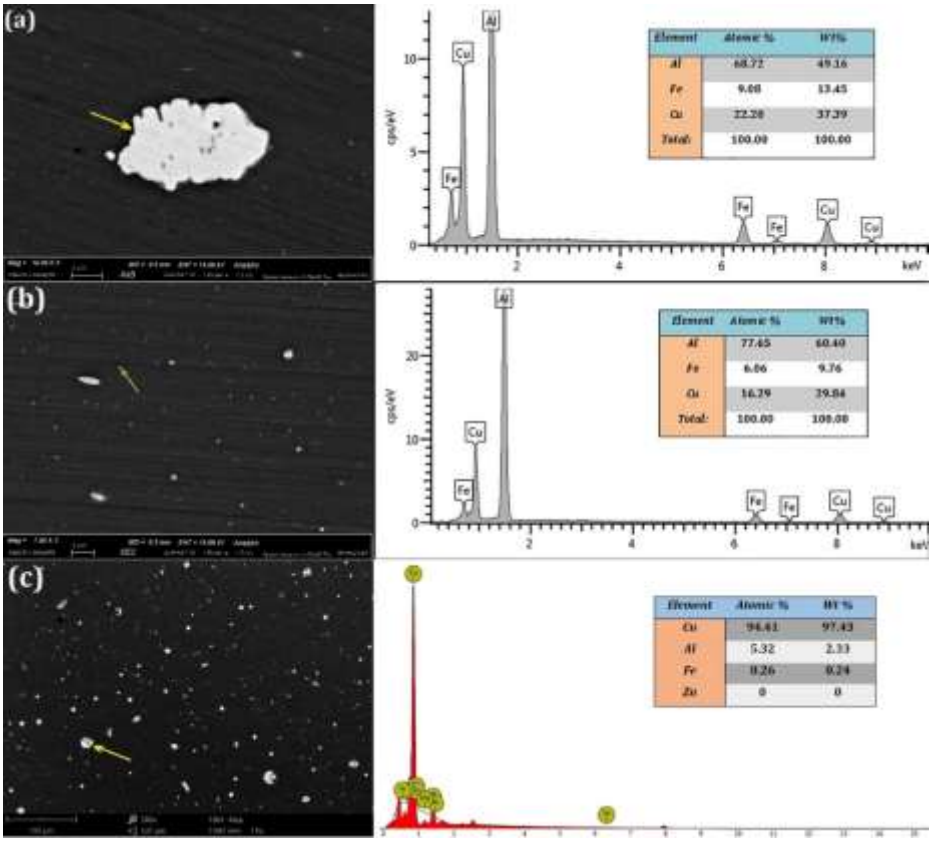

Fig. 6: FE-SEM images and related EDS provided from intermetallic particles in (a) AA2198 base metal, (b) SZ of AA2198, and (c) SZ of AA7475.

Figs. 6(a-c) show the morphology, size distribution, and chemical composition of the particles in base metals and SZ of dissimilar joint. It is clear that particles in SZ were finer compared with the base metals. The chemical composition of the particles provided by EDS analysis approved the XRD outputs. Because in AA2198, Wt% of Al was 49.16% and Wt% of Cu/Fe was about 50.84%, which implies the formation of the AlCu compound. Meanwhile, Wt% of Al in fine particles of the SZ was twice the Cu/Fe, which points to precipitation of $Al_2(Cu,Fe)$ particles. This result was completely in accordance with the obtained results by XRD. EDS analysis taken from particles in SZ of AA7475 revealed that they were enriched from the Cu. Supplementary investigation on the evolved precipitates in SZ performed using backscatter FE-SEM map elemental analysis (Fig. 7).

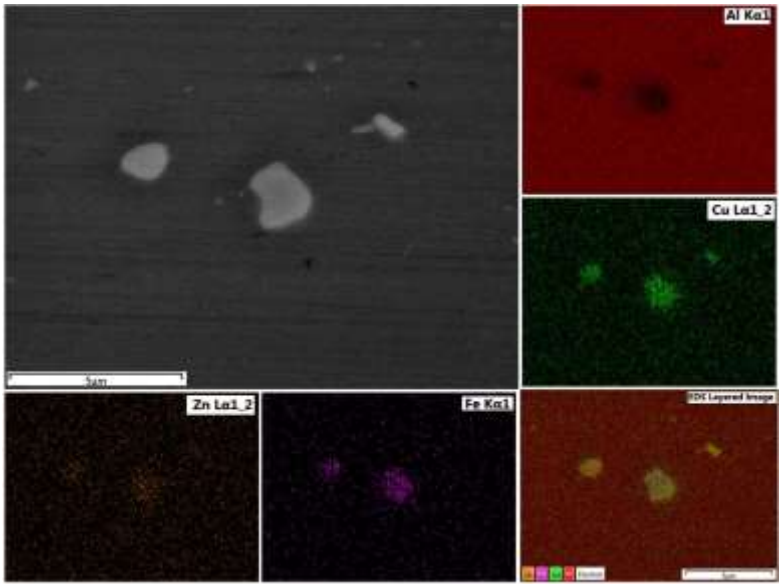

Fig. 7: Backscatter FE-SEM elemental map view indicating the distribution of main constituent elements in the SZ of FSWed AA7475-AA2198.

As can be seen, Cu and Fe were the substantial contributing elements of the analyzed particles in SZ that validates the EDS and XRD outputs. Likewise, a small amount of Zn was also detected in particles, which probably diffused to SZ from AA7475. It is proved that generally, the main strengthening phases in AA7475 are $MgZn_2$ (η or η') and $CuMgAl_2$ (S) [64].

Stereo micrograph presenting different regions in dissimilar welding of AA2198 to AA7475 and the hardness variation across the weld line in similar and dissimilar states is shown in Fig. 8.

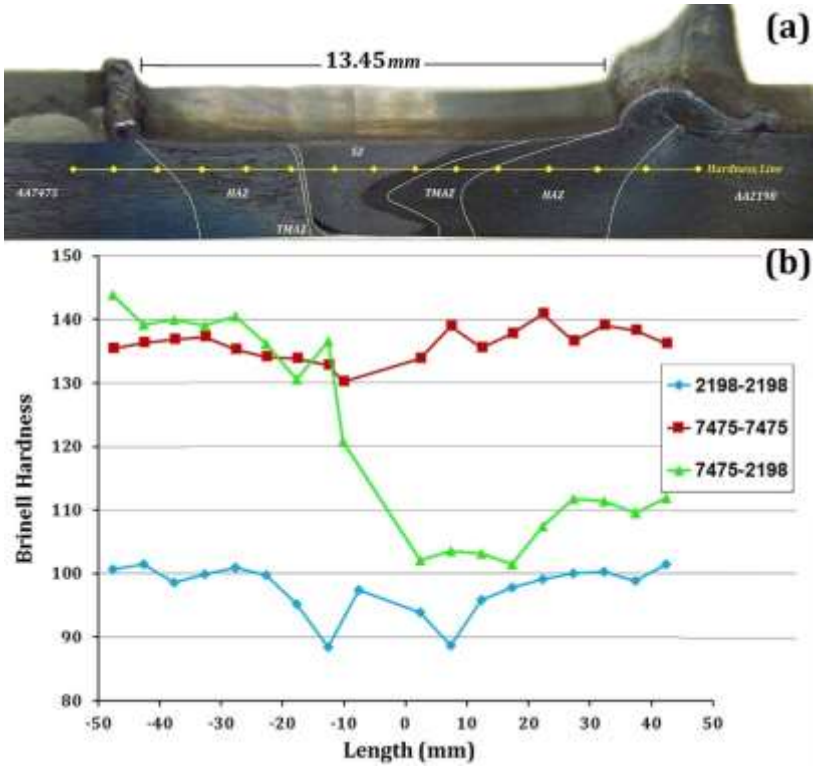

Fig. 8: Macro-image showing different zones in dissimilar weld (a) and variation of Brinell hardness in similar and dissimilar states (b) in FSWed AA7475 and AA2198 sheets.

As shown, in similar welded AA7475 sheets, hardness was rather homogeneous across the joint, ranging from 130 to 140 HB. Except the remarkable hardness decline in TMAZ, similar welding of AA2198 sheets also induced a uniform hardness distribution (about 100 HB). Due to the grain refinement and distribution of fine precipitates in SZ, the center of the weld line showed higher hardness than TMAZ. The hardness profile of a dissimilar joint of AA7475-AA2198 showed that apart from strength depression in TMAZ, the hardness of AA7475 was higher because of the synergistic effect of finer grain and small precipitates strengthening. Analysis of DSC taken from different sections of the similar welded AA2198, similar welded AA7475 and dissimilar welding between AA7475 and AA2198 are shown in Figs. 9(a), 9(b) and 9(c), respectively.

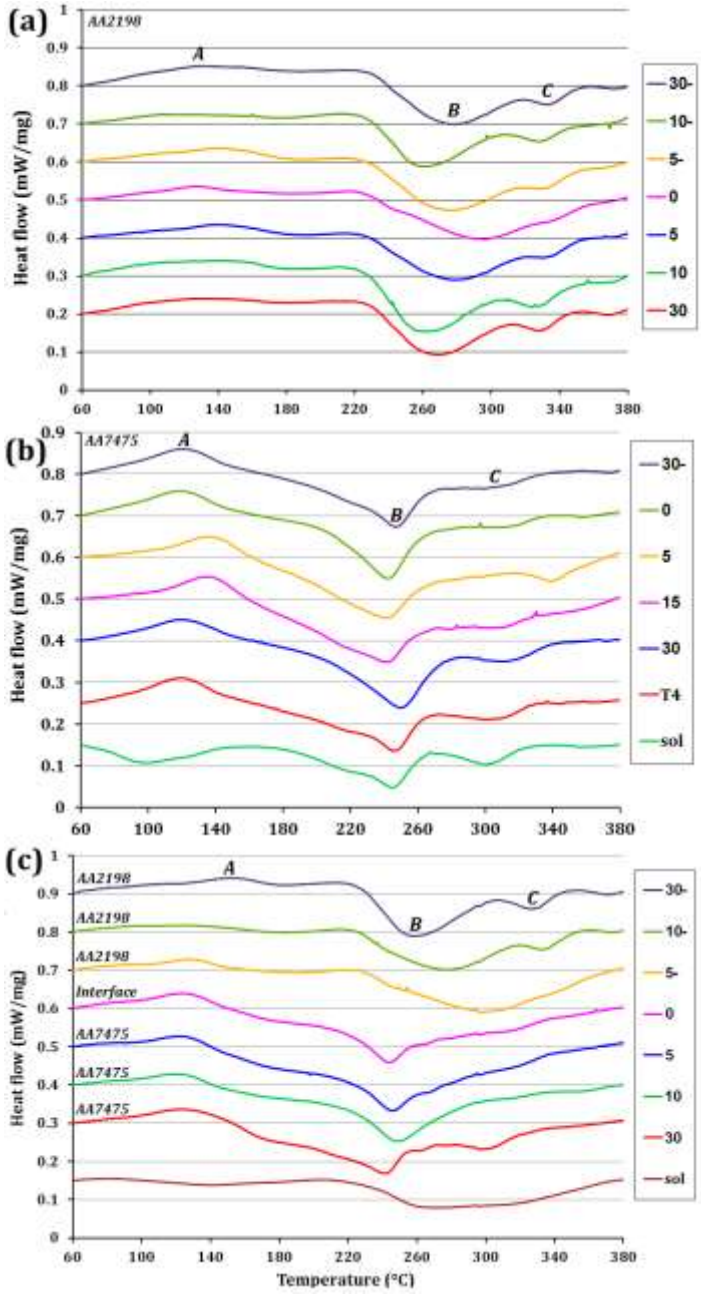

Fig. 9: DSC curves of the samples sectioned from different locations across the AA2198-AA2198 (a), AA7475-AA7475 (b) and AA2198-AA7475 joints. Numbers point to distance from the welding interface.

Accordingly, during the heating of AA2198, a prominent peak at 260 °C and a shallow peak around 330 °C have emerged (**Fig. 9a**). In 2xxx Al alloys, often two exothermic peaks of precipitation and three endothermic peaks of dissolution appears that imply on formation and dissolution of GPB zones and intermetallic phases, respectively **[65, 66]**. The dissolution of the GPB zone appeared as a shallow peak on DSC curves (point A). As can be seen, approaching to the welding center from both sides was accompanied by a slight shift in precipitation peak to higher temperatures (point B). It might arise from releasement of residual stress remained from pre-straining through welding heat. Besides, the third peak (point C) was removed in the welding center, which could be attributed to the absence of a certain phase in SZ compared to the base metal. Based on DSC curves of FSWed AA7475-AA7475 from base metal to SZ (**Fig. 9b**) solubilized specimen demonstrated an exothermic peak close to 100 °C after quenching due to GP zone formation. In the following, two subsequent exothermic peaks were emerged on the DSC curve around 250 °C and 300 °C, which probably were originated from the precipitation of η and η' phases. During the natural aging, the first exothermic peak was omitted and an endothermic peak altered around 120 °C owing to the dissolution of GP zones. Similar observation is also reported on AA7075 **[67]**. A comparison of DSC curves from base to SZ in welded sheets indicated that the nugget and base metal experienced similar phase transformations. However, emersion of an exothermic peak at 340 °C in TMAZ suggests that some particles were formed there. Furthermore, the maximum peak depth at 250 °C was related to the welding center, which implies on precipitation of more particles in the SZ. GP dissolution in nugget took place at 120 °C. By getting away from the SZ, endothermic peaks in HAZ and TMAZ were shifted to the higher temperatures. However, exothermic precipitation of η phase occurred at a rather lower temperature. Fuller et al. **[68]** also reported similar results during the aging of AA7XXX and attributed the observed peak at 120 °C to dissolution of GP(I) zones and the other peak at 140 °C to dissolution of GP(II) zones, respectively. It suggests that FSW has no significant effect on the precipitation of the η phase. Because the peak of η dissolution did not observe and the precipitation had similar enthalpy in different welding zones. According to the DSC analysis of dissimilar joint between AA7475 and AA2198 from the base to weld (**Fig. 9c**), the general trend of DSC curves for the dissimilar joint was alike with those welded as similar. As shown, by approaching the welding interface, endothermic peak A was shifted to lower temperatures, exothermic peak B became shallower and was displaced to the higher temperatures and peak C gradually have been disappeared. The obtained results revealed that in AA2198 side of the dissimilar joint, the accumulation of particles in SZ was lower than the base metal. Whereas in AA7475, base metal had similar characteristics with the SZ. As can be seen, solution treatment of the welded sheets in elevated temperatures dissolved most of the particles, and any highlight phase transformation did not emerge in the DSC curve of the solution treated sample.

Solution treatment

As aforementioned, a wide range of time (5 min to 8 h) and temperature (450-600 °C) for solution treatment of FSWed AA2XXX and AA7XXX sheets were introduced in the literature. In order to find the optimum treatment condition, at first, samples were annealed at 560 °C for 1 h to dissolve most of the particles and inclusions. The microstructure of dissimilarly welded AA2198-AA7475 after solution-treatment at 560 °C is presented in Fig. 10.

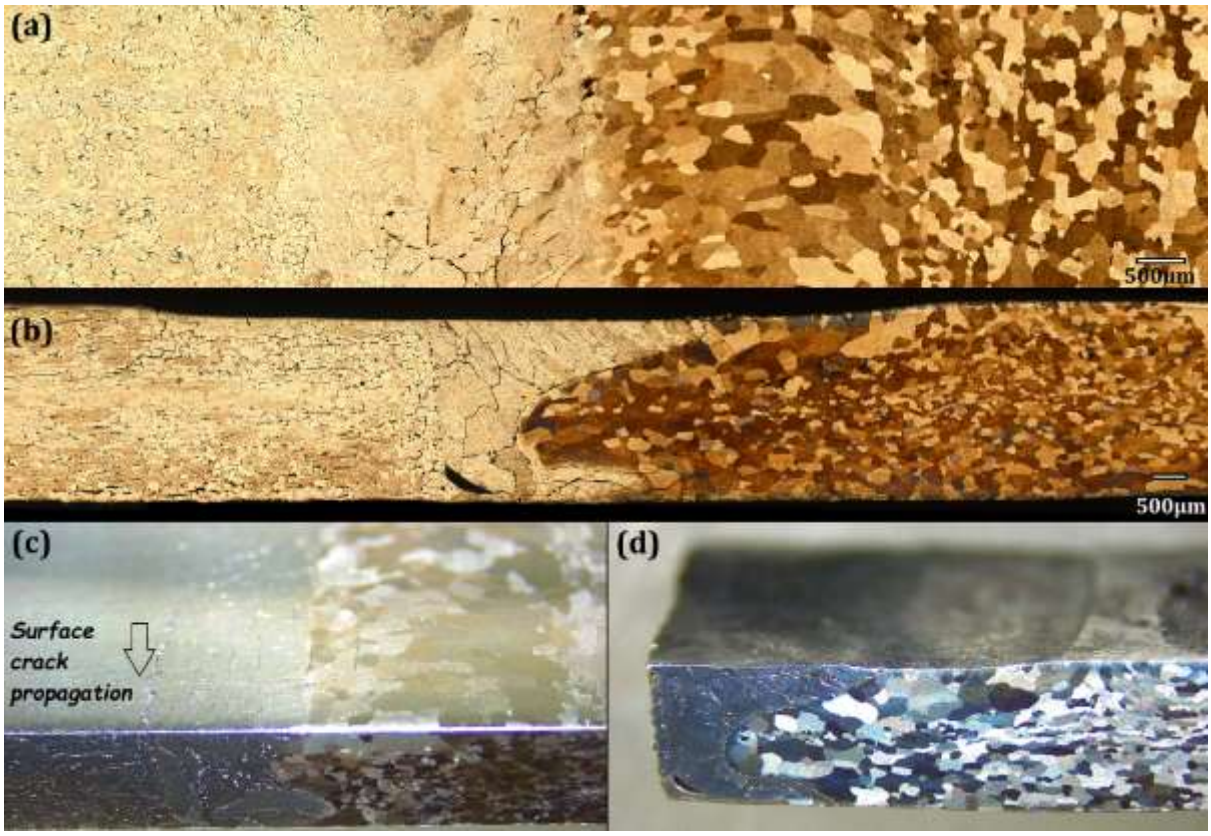

Fig. 10: Microstructure of FSWed AA7475-AA2198-T3 after solution-treatment at 560 °C for 1 h in surface (a) and cross-section (b) of the sample, and stereo micrograph of crack propagation (c) and failure of the joint (d) from TMAZ of AA7475.

As can be seen, annealing at 560 °C for 1 h completely eliminated the welding history. Comparison of Figs. 10(a) and 10(b), which are provided from surface and cross-section of solution treated sample indicated that unlike the as-weld state, maximum grain growth has occurred in SZ and TMAZ. However, the formation of some cracks in SZ and TMAZ of AA7475 that were propagated parallel to the welding junction (Fig. 10c) debilitated the TMAZ and resulted in the failure of the weld from this point (Fig. 10d). Analysis of the fracture surface revealed that applying a temperature higher than 550 °C for a long time led to the formation of Cu-rich compounds in the SZ and TMAZ (Fig. 11a) and intensive grain growth (Fig. 11b) in these areas. Such disbanding due to the formation of Cu compounds having a weakening effect has also observed on Ti-Cu joints [69].

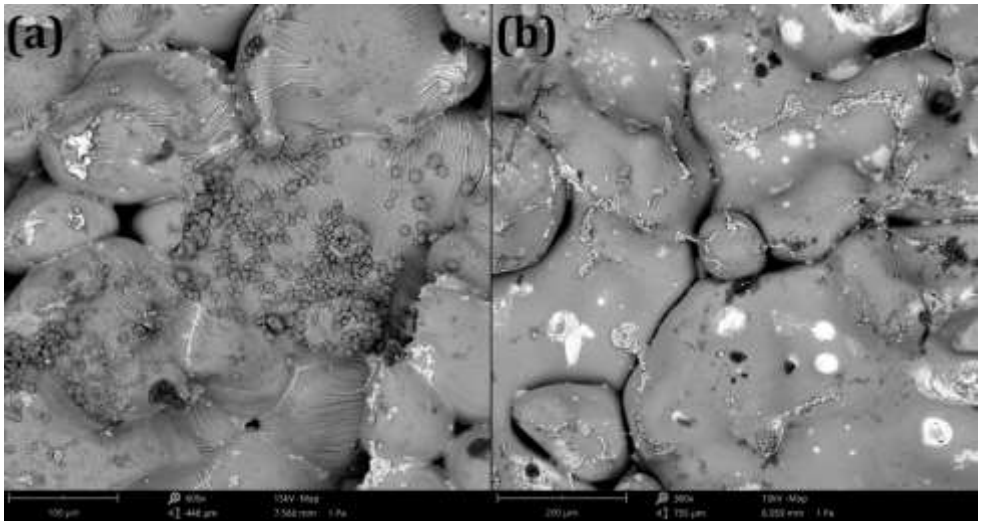

Fig. 11: Formation of the IM phases in grain boundaries after solution treatment at 560 °C for 1 h.

Due to the destructive consequence of high annealing time and temperature, other solution treatment procedures were examined. For this purpose, samples were annealed at 480 °C for 30 to 90 min (Fig. 12) and at 540 °C for 10 to 30 min (Fig. 13), respectively.

Fig. 12: Solution treatment of dissimilar joint of AA7475-AA2198 at 480 °C for 30 to 90 min.

As illustrated, during annealing at 480 °C recrystallization of the new grains began from the weld surface. In the following, grains were elongated toward the bottom of SZ, and grain growth was

started from the center of SZ. However, during annealing at 480 °C, SZ of AA7475 was entirely recrystallized, but still notable parts of TMAZ in AA2198 were not recrystallized even after 90 min solution treatment. Hence, annealing at higher temperatures has been examined.

Fig. 13: Solution treatment of dissimilar joint of AA7475-AA2198 at 540 °C for 10 to 30 min.

The comparison of the microstructural changes during the annealing at 540 °C with obtained structures during annealing at 480 °C indicated that higher temperatures could increase the nucleation sites during the recrystallization. As a result, finer grains could germinate from stress localization points, i.e., SZ and TMAZ. According to Fig. 13, after 30 min annealing at 540 °C, almost whole of SZ and TMAZ on both sides were recrystallized. However, parts of the initially recrystallized grains in the welding surface were grown. Hence, all the dissimilar welded specimens were solution treated at 540 °C for 30 min before aging.

Aging

Common standard aging procedure for AA2198 alloy is T8 temper as isothermal treatment at 155 °C for 14 h [70]. On the other hand, for the AA7475 sheets, two types of heat treatments were introduced. Often for the standard aging, T6xx treatment was employed and when an over aging could improve the exfoliation or stress corrosion resistance, T76xx and T73xx were applied by

the researchers. Usually, these treatments have been performed in two stages. In the first step, samples underwent short-term aging at 100-120 °C, and in the second step, were subjected to long-term aging at 155-170 °C.

To investigate the effect of STA on the mechanical strength of the studied alloys, firstly AA2198-AA2198 and AA7475-AA7475 similar joints were heat-treated at temperatures of 155 °C and 170 °C. Variation of hardness in similar FSWed sheets as a function of aging time at 155 °C is depicted in Fig. 14.

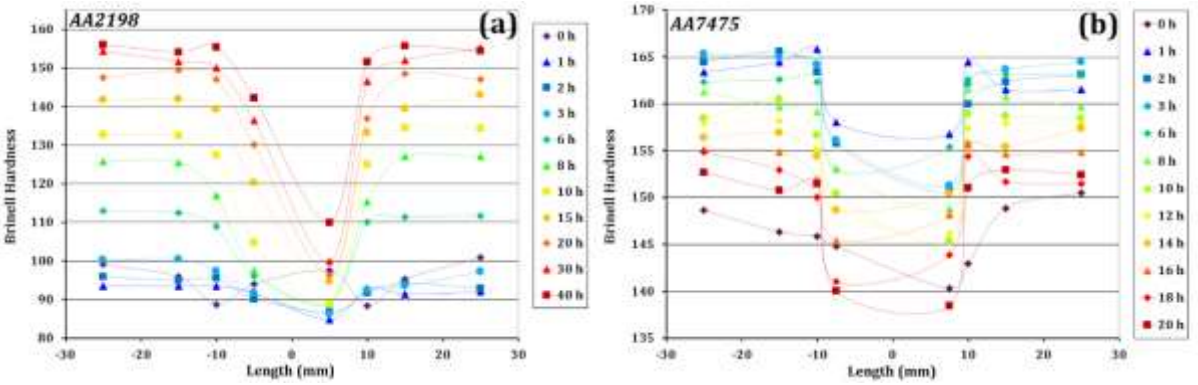

Fig. 14: Transversal hardness profile in AA2198-AA2198 joint after aging at 155 °C (a) and in aged AA7475-AA7475 weld after aging at 170 °C in different periods after 3h annealing at 120 °C.

As can be seen, aging up to 3 h had no significant effect on similar welded of AA2198 sheets. But longer aging gradually increased the hardness while a substantial difference between the SZ and base metal was established. In particular, base metal ever showed higher hardness values than the weld zone during the long-term aging. It could be attributed to the precipitation coarsening and partial grain growth in SZ. Based on the hardness profile in the transverse section of the similar FSWed AA7475 sheets (Fig. 14b), increasing the aging time had a destructive effect on hardness due to overaging drawbacks. In the meantime, hardness value in advancing and retreating sides had close values. Hardness variation as a function of aging time in different distances from the SZ is measured and the results are presented in Figs. 15 (a) and 15 (b).

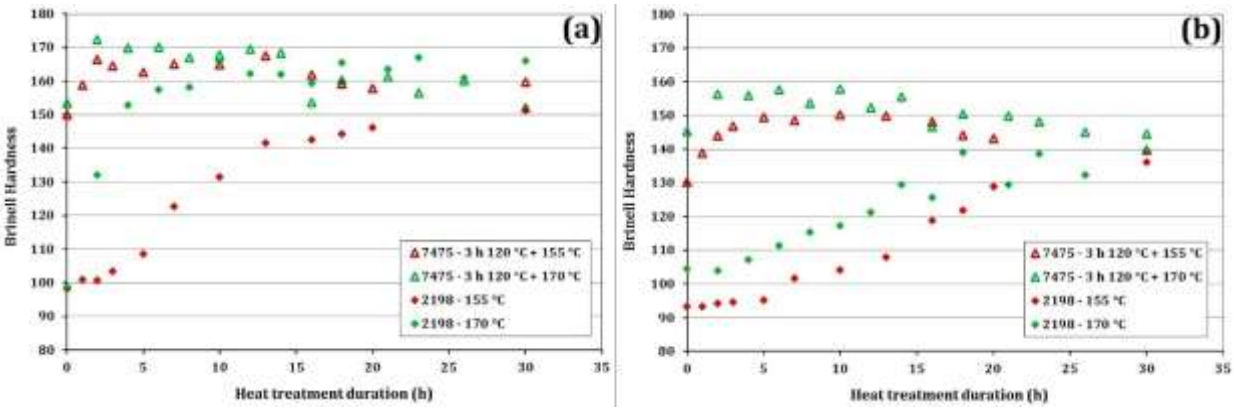

Fig. 15: Variation of hardness as a function of aging time for the 2198-7475 weld at 155 °C and 170 °C in base metal (a) and HAZ/TMAZ interface (b) of the AA2198 and AA7475.

Comparison of Figs. 15 (a) and 15 (b) revealed that aging at 170 °C induced higher improvement in the hardness value in both base metal and the HAZ/TMAZ interface, particularly in AA2198 side. Although aging longer than 20 h eventuated in hardness attenuation in the AA7475. The enhancement of the mechanical strength in AA2198 side and attenuation in hardness value in the AA7475 side can be attributed to nucleation of second-phase particles and coarsening of the precipitates, respectively. Because due to the low temperature for aging, even long-term aging could on remarkably impress the grain size of the welded sheets. The corresponding hardness profile across the weld line after two-step aging at 170 °C is depicted in Fig. 16.

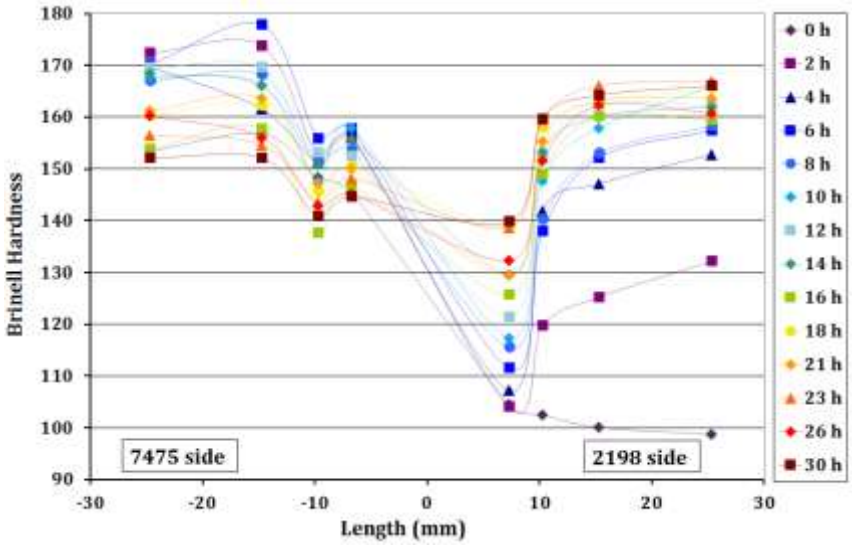

Fig. 16: Effect of aging time at 170 °C after primary treatment at 120 °C for 3h on the hardness profile of AA2198-AA7475 weld line.

The most highlight advantage of aging up to about 20 h was the hardness trade-off in both sides of the weld line and reaching to a uniform strength. Aging below 18 h however could improve the hardness in AA2198 side to the desired level, but still, the TMAZ of AA2198 was the weakest point along the joint. In the meantime, aging longer than 21h led to a significant drop in hardness in AA7475 side which probably was due to over-aging and precipitate coarsening. The optimum aging condition would be the balance point between the hardness decline in the AA7475 side and the hardness enhancement in AA2198 side. Hence, despite the significant difference between the hardness values in two sides of the weld line at the beginning of aging, after about 18-21 h aging, the weld line was reached to a uniform strength without any defects formation throughout the joined sheets.

Concluding remarks

In the current study, aerospace aluminum alloys of 2198-T3 and 7475-W were joined together via friction stir welding (FSW) technique. To optimize the weld properties, samples underwent STA treatment employing different combinations of solution treatment and aging, and the

microstructure and hardness variation were evaluated. The most highlight achievements of this research can be summarized as follows:

- Microstructural observations revealed that during the FSW process, the finest grains were formed in the SZ and particularly the surface of the joint, which was in direct touch with the rotary shoulder. During the solution treatment, recrystallization began from such stress localization points followed by an abnormal grain growth.
- OM analysis of the solution treated samples at 480 °C and 540 °C indicated that solution treatment at 540 °C for 30 min pulled the trigger of the recrystallization from multiple sites and created finer grains. Likewise, by annealing at 480 °C, recrystallization was started from the surface and the grains were gradually grown toward the center of SZ.
- Comparison of phase transformations by EDS, FE-SEM, XRD, and DCS proved that AA2198 was more susceptible to precipitation. Such characteristics validated by more peaks in DSC curves implying on phase transformations, diverse particles detected by XRD and enrichment of the particles in SZ from the elements diffused from base metals to the SZ.
- Regardless of similar/dissimilar welding, the hardness in SZ was lower than the parent metals. The minimum hardness obtained in the HAZ/TMAZ interface. Such a hardness depression could attribute to the coarsening of the precipitates in this area.
- Generally, imposing the STA to AA2198 samples improved their hardness, while it had a destructive effect on AA7475. Hence, in similar joints, aging could be beneficial for AA2198 and was detrimental to the AA7475. In the dissimilar state, aging up to about 20h induced the uniform hardness profile, while longer aging led to hardness attenuation.

Acknowledgments

The authors wish to thanks the MR&D (Manufacturing Research and Development) of Alenia Aeronautica Co. (Pomigliano d'Arco – Italy) for supplying the examined aluminum sheets.

References

[1] N. Nayan, M. Yadava, R. Sarkar, S.N. Murty, N. Gurao, S. Mahesh, M. Prasad, I. Samajdar, Microstructure and tensile response of friction stir welded Al–Cu–Li (AA2198-T8) alloy, Materials Characterization, 159 (2020) 110002.

[2] H. Shirazi, S. Kheirandish, H. Pouraliakbar, Employing hooking and effective sheet thickness to achieve optimum failure load in lap joints of friction stir welded AA5456 aluminum, Theoretical and Applied Fracture Mechanics, 105 (2020) 102423.

[3] Z. Gao, M. Chen, W.G. Guo, J. Li, Tool Wear Characterization and Monitoring with Hierarchical Spatio-Temporal Models for Micro-Friction Stir Welding, Journal of Manufacturing Processes, (2020).

[4] M.R. Jandaghi, H. Pouraliakbar, A. Saboori, Effect of second-phase particles evolution and lattice transformations while ultrafine graining and annealing on the corrosion resistance and electrical conductivity of Al–Mn–Si alloy, Materials Research Express, 6 (2019) 1065d1069.

[5] M.R. Jandaghi, A. Saboori, G. Khalaj, M.K.G. Shiran, Microstructural Evolutions and its Impact on the Corrosion Behaviour of Explosively Welded Al/Cu Bimetal, Metals, 10 (2020) 634.
[6] M.R. Azad, A. Ghasemi, H. Pouraliakbar, M.R. Jandaghi, On the Al/Cu Dissimilar Joints Produced Through Simple Cold Compression, Transactions of the Indian Institute of Metals, 68 (2015) 991-998.
[7] M.K.G. Shiran, G. Khalaj, H. Pouraliakbar, M.R. Jandaghi, A.S. Dehnavi, H. Bakhtiari, Multilayer Cu/Al/Cu explosive welded joints: Characterizing heat treatment effect on the interface microstructure and mechanical properties, Journal of Manufacturing Processes, 35 (2018) 657-663.
[8] N. Kashaev, V. Ventzke, G. Çam, Prospects of laser beam welding and friction stir welding processes for aluminum airframe structural applications, Journal of Manufacturing Processes, 36 (2018) 571-600.
[9] G. Çam, G. İpekoğlu, Recent developments in joining of aluminum alloys, The International Journal of Advanced Manufacturing Technology, 91 (2017) 1851-1866.
[10] G. Çam, Friction stir welded structural materials: beyond Al-alloys, Int. Mater. Rev., 56 (2011) 1-48.
[11] G. Çam, S. Mistikoglu, Recent developments in friction stir welding of Al-alloys, Journal of Materials Engineering and Performance, 23 (2014) 1936-1953.
[12] A. Heidarzadeh, H. Pouraliakbar, S. Mahdavi, M.R. Jandaghi, Ceramic nanoparticles addition in pure copper plate: FSP approach, microstructure evolution and texture study using EBSD, Ceramics International, 44 (2018) 3128-3133.
[13] T. Küçükömeroğlu, E. Şentürk, L. Kara, G. İpekoğlu, G. Çam, Microstructural and mechanical properties of friction stir welded nickel-aluminum bronze (NAB) alloy, Journal of Materials Engineering and Performance, 25 (2016) 320-326.
[14] G. Çam, S. Mistikoglu, M. Pakdil, Microstructural and mechanical characterization of friction stir butt joint welded 63% Cu-37% Zn brass plate, Weld. J, 88 (2009) 225-232.
[15] L. Wu, X. Hu, X. Zhang, Y. Li, Z. Ma, X. Ma, B. Xiao, Fabrication of high-quality Ti joint with ultrafine grains using submerged friction stirring technology and its microstructural evolution mechanism, Acta Materialia, 166 (2019) 371-385.
[16] G. Li, L. Zhou, S. Luo, F. Dong, N. Guo, Microstructure and mechanical properties of bobbin tool friction stir welded ZK60 magnesium alloy, Materials Science and Engineering: A, (2020) 138953.
[17] D. Sunilkumar, S. Muthukumaran, M. Vasudevan, M. Reddy, Tool rotational speed variant response on the evolution of microstructure and its significance on mechanical properties of friction stir welded 9Cr-1Mo steel, Journal of Materials Processing Technology, 278 (2020) 116536.
[18] A. Amirafshar, H. Pouraliakbar, Effect of tool pin design on the microstructural evolutions and tribological characteristics of friction stir processed structural steel, Measurement, 68 (2015) 111-116.
[19] T. Küçükömeroğlu, S.M. Aktarer, G. İpekoğlu, G. Çam, Microstructure and mechanical properties of friction-stir welded St52 steel joints, International Journal of Minerals, Metallurgy, and Materials, 25 (2018) 1457-1464.
[20] T. Küçükömeroğlu, S.M. Aktarer, G. İpekoğlu, and G. Çam, Mechanical properties of friction stir welded St 37 and St 44 steel joints, Materials Testing, 60 (12) (2018) 1163-1170.
[21] A. Günen, E. Kanca, M. Demir, F. Çavdar, S. Mistikoğlu, G. and Çam, Microstructural and mechanical properties of friction stir welded pure lead, Indian Journal of Engineering & Materials Sciences, 25 (1) (2018) 26-32.

[22] H. Deng, Y. Chen, S. Li, C. Chen, T. Zhang, M. Xu, D. Ji, Microstructure, mechanical properties and transformation behavior of friction stir welded Ni50. 7Ti49. 3 alloy, Materials & Design, (2020) 108491.
[23] S. Delijaicov, P.A.d.O. Silva, H.B. Resende, M.H.F. Batalha, Effect of weld parameters on residual stress, hardness and microstructure of dissimilar AA2024-T3 and AA7475-T761 friction stir welded joints, Materials Research, 21 (2018).
[24] Q. Chu, W. Li, H. Hou, X. Yang, A. Vairis, C. Wang, W. Wang, On the double-side probeless friction stir spot welding of AA2198 Al-Li alloy, Journal of Materials Science & Technology, 35 (2019) 784-789.
[25] C. de SC Machado, R.E. Klumpp, V.H. Ayusso, U. Donatus, M.X. Milagre, J.V. de S. Araujo, G.A. F. Machado, I. Costa, Effect of surface treatments on the localized corrosion resistance of the AA2198-T8 aluminum lithium alloy welded by FSW process, Surf. Interface Anal., 51 (2019) 1231-1239.
[26] G. İpekoğlu, B. Gören Kıral, S. Erim, G. Çam, Investigation of the effect of temper condition on friction stir weldability of AA7075 Al-alloy plates, Mater Technol, 46 (2012) 627-632.
[27] P. Niu, W. Li, N. Li, Y. Xu, D. Chen, Exfoliation corrosion of friction stir welded dissimilar 2024-to-7075 aluminum alloys, Materials Characterization, 147 (2019) 93-100.
[28] C. Zhang, G. Huang, Y. Cao, Y. Zhu, Q. Liu, On the microstructure and mechanical properties of similar and dissimilar AA7075 and AA2024 friction stir welding joints: effect of rotational speed, Journal of Manufacturing Processes, 37 (2019) 470-487.
[29] G. Çam, G. İpekoğlu, H. Tarık Serindağ, Effects of use of higher strength interlayer and external cooling on properties of friction stir welded AA6061-T6 joints, Sci. Technol. Weld. Joining, 19 (2014) 715-720.
[30] M. Reimann, J. Goebel, T.M. Gartner, J.F. dos Santos, Refilling termination hole in AA 2198–T851 by refill friction stir spot welding, Journal of Materials Processing Technology, 245 (2017) 157-166.
[31] J. Goebel, M. Reimann, A. Norman, J.F. dos Santos, Semi-stationary shoulder bobbin tool friction stir welding of AA2198-T851, Journal of Materials Processing Technology, 245 (2017) 37-45.
[32] F. Wang, W. Li, J. Shen, S. Hu, J. Dos Santos, Effect of tool rotational speed on the microstructure and mechanical properties of bobbin tool friction stir welding of Al–Li alloy, Materials & Design, 86 (2015) 933-940.
[33] M.X. Milagre, N.V. Mogili, U. Donatus, R.A. Giorjão, M. Terada, J.V.S. Araujo, C.S. Machado, I. Costa, On the microstructure characterization of the AA2098-T351 alloy welded by FSW, Materials Characterization, 140 (2018) 233-246.
[34] J. Entringer, M. Reimann, A. Norman, J.F. dos Santos, Influence of Cu/Li ratio on the microstructure evolution of bobbin-tool friction stir welded Al–Cu–Li alloys, Journal of Materials Research and Technology, 8 (2019) 2031-2040.
[35] S.N.J. Reddy, R. Sathiskumar, K.G. Kumar, S. Jerome, A.V. Jebaraj, N. Arivazhagan, M. Manikandan, Friction based joining process for high strength aerospace aluminium alloy, Materials Research Express, 6 (2019) 0865a0863.
[36] T. Kalashnikova, S. Tarasov, A. Eliseev, A. Fortuna, Towards the problem of forming full strength welded joints on aluminum alloy sheets. Part II: AA7475, in: AIP Conf. Proc., AIP Publishing LLC, 2016, pp. 020080.
[37] A. Jacob, S. Maheshwari, A.N. Siddiquee, N. Gangil, Improvements in strength and microstructural behaviour of friction stir welded 7475 aluminium alloy using in-process cooling, Materials Research Express, 5 (2018) 076518.

[38] R.K. Gupta, H. Das, T.K. Pal, Influence of processing parameters on induced energy, mechanical and corrosion properties of FSW butt joint of 7475 AA, Journal of materials engineering and performance, 21 (2012) 1645-1654.
[39] P. Goel, N.Z. Khan, Z.A. Khan, A. Ahmari, N. Gangil, M.H. Abidi, A.N. Siddiquee, Investigation on material mixing during FSW of AA7475 to AISI304, Materials and Manufacturing Processes, 34 (2019) 192-200.
[40] M. Kadlec, R. Růžek, L. Nováková, Mechanical behaviour of AA 7475 friction stir welds with the kissing bond defect, Int. J. Fatigue, 74 (2015) 7-19.
[41] N.Z. Khan, A.N. Siddiquee, Z.A. Khan, A.K. Mukhopadhyay, Mechanical and microstructural behavior of friction stir welded similar and dissimilar sheets of AA2219 and AA7475 aluminium alloys, Journal of Alloys and Compounds, 695 (2017) 2902-2908.
[42] T. Senthilnathan, K. Balachandar, FRICTION STIR WELDING OF AA7475 HYBRID COMPOSITES, Technology, 9 (2018) 582-588.
[43] C. Badini, M. Pavese, P. Fino, S. Biamino, Laser beam welding of dissimilar aluminium alloys of 2000 and 7000 series: effect of post-welding thermal treatments on T joint strength, Sci. Technol. Weld. Joining, 14 (2009) 484-492.
[44] G. İpekoğlu, G. Çam, Effects of initial temper condition and postweld heat treatment on the properties of dissimilar friction-stir-welded joints between AA7075 and AA6061 aluminum alloys, Metallurgical and Materials Transactions A, 45 (2014) 3074-3087.
[45] G. İpekoğlu, S. Erim, G. Çam, Effects of temper condition and post weld heat treatment on the microstructure and mechanical properties of friction stir butt-welded AA7075 Al alloy plates, The International Journal of Advanced Manufacturing Technology, 70 (2014) 201-213.
[46] G. Khalaj, H. Pouraliakbar, M.R. Jandaghi, A. Gholami, Microalloyed steel welds by HF-ERW technique: novel PWHT cycles, microstructure evolution and mechanical properties enhancement, International Journal of Pressure Vessels and Piping, 152 (2017) 15-26.
[47] X. Tao, Y. Chang, Y. Guo, W. Li, M. Li, Microstructure and mechanical properties of friction stir welded oxide dispersion strengthened AA6063 aluminum matrix composites enhanced by post-weld heat treatment, Materials Science and Engineering: A, 725 (2018) 19-27.
[48] A. Rodríguez, A. Calleja, L.N. López de Lacalle, O. Pereira, H. González, G. Urbikain, J. Laye, Burnishing of FSW Aluminum Al–Cu–Li Components, Metals, 9 (2019) 260.
[49] H. Sidhar, R.S. Mishra, A.P. Reynolds, J.A. Baumann, Impact of thermal management on post weld heat treatment efficacy in friction stir welded 2050-T3 alloy, Journal of Alloys and Compounds, 722 (2017) 330-338.
[50] R. Kosturek, L. Śnieżek, M. Wachowski, J. Torzewski, The influence of post-weld heat treatment on the microstructure and fatigue properties of Sc-modified AA2519 friction stir-welded joint, Materials, 12 (2019) 583.
[51] Y. Lin, C. Lu, C. Wei, Z. Zheng, Influences of Friction Stir Welding and Post-Weld Heat Treatment on Al–Cu–Li Alloy, Advanced Engineering Materials, 20 (2018) 1700652.
[52] B. Malard, F. De Geuser, A. Deschamps, Microstructure distribution in an AA2050 T34 friction stir weld and its evolution during post-welding heat treatment, Acta Materialia, 101 (2015) 90-100.
[53] J. Zhang, X. Feng, J. Gao, H. Huang, Z. Ma, L. Guo, Effects of welding parameters and post-heat treatment on mechanical properties of friction stir welded AA2195-T8 Al-Li alloy, Journal of Materials Science & Technology, 34 (2018) 219-227.
[54] Z. Zhang, B. Xiao, Z. Ma, Enhancing mechanical properties of friction stir welded 2219Al-T6 joints at high welding speed through water cooling and post-welding artificial ageing, Materials Characterization, 106 (2015) 255-265.

[55] S. Rajesh, V. Badheka, Influence of heat input/multiple passes and post weld heat treatment on strength/electrochemical characteristics of friction stir weld joint, Materials and Manufacturing Processes, 33 (2018) 156-164.
[56] N.Z. Khan, A.N. Siddiquee, Z.A. Khan, M. Ubaid, D. Bajaj, M. Atif, A. Khan, Microstructure evolution of friction stir welded dissimilar aerospace aluminium alloys, in: IOP Conference Series: Materials Science and Engineering, IOP Publishing, 2018, pp. 012002.
[57] K. Lv, C. Zhu, J. Zheng, X. Wang, B. Chen, Precipitation of T 1 phase in 2198 Al–Li alloy studied by atomic-resolution HAADF-STEM, J. Mater. Res., 34 (2019) 3535-3544.
[58] B. Decreus, A. Deschamps, P. Donnadieu, Understanding the mechanical properties of 2198 Al-Li-Cu alloy in relation with the intra-granular and inter-granular precipitate microstructure, in: Journal of Physics: Conference Series, IOP Publishing, 2010, pp. 012096.
[59] J. Tian, Y. Zhao, H. Hou, B. Wang, The effect of alloying elements on the structural stability, mechanical properties, and Debye temperature of Al3Li: A first-principles study, Materials, 11 (2018) 1471.
[60] Y. Peng, A. Chen, L. Zhang, W. Liu, G. Wu, Effect of solution treatment on microstructure and mechanical properties of cast Al–3Li–1.5 Cu–0.2 Zr alloy, J. Mater. Res., 31 (2016) 1124-1132.
[61] M.R. Jandaghi, H. Pouraliakbar, Elucidating the microscopic origin of electrochemical corrosion and electrical conductivity by lattice response to severe plastic deformation in Al-Mn-Si alloy, Materials Research Bulletin, 108 (2018) 195-206.
[62] H. Pouraliakbar, M.R. Jandaghi, S.J.M. Baygi, G. Khalaj, Microanalysis of crystallographic characteristics and structural transformations in SPDed Al Mn Si alloy by dual-straining, Journal of Alloys and Compounds, 696 (2017) 1189-1198.
[63] M.R. Jandaghi, H. Pouraliakbar, G. Khalaj, M.-J. Khalaj, A. Heidarzadeh, Study on the post-rolling direction of severely plastic deformed Aluminum-Manganese-Silicon alloy, Archives of Civil and Mechanical Engineering, 16 (2016) 876-887.
[64] A. Bhagavatam, A. Ramakrishnan, V. Adapa, G. Dinda, Laser metal deposition of aluminum 7075 alloy, Int. J. Mater. Sci. Res, 1 (2018) 50-55.
[65] Q. Chu, X. Yang, W. Li, Y. Zhang, T. Lu, A. Vairis, W. Wang, On visualizing material flow and precipitate evolution during probeless friction stir spot welding of an Al-Li alloy, Materials Characterization, 144 (2018) 336-344.
[66] H. Sidhar, R.S. Mishra, Aging kinetics of friction stir welded Al-Cu-Li-Mg-Ag and Al-Cu-Li-Mg alloys, Materials & Design, 110 (2016) 60-71.
[67] A. Ghosh, M. Ghosh, G. Shankar, On the role of precipitates in controlling microstructure and mechanical properties of Ag and Sn added 7075 alloys during artificial ageing, Materials Science and Engineering: A, 738 (2018) 399-411.
[68] C.B. Fuller, M.W. Mahoney, M. Calabrese, L. Micona, Evolution of microstructure and mechanical properties in naturally aged 7050 and 7075 Al friction stir welds, Materials Science and Engineering: A, 527 (2010) 2233-2240.
[69] Y.K. Kim, H. Pouraliakbar, S.I. Hong, Effect of interfacial intermetallic compounds evolution on the mechanical response and fracture of layered Ti/Cu/Ti clad materials, Materials Science and Engineering: A, 772 (2020) 138802.
[70] C. Gao, Y. Ma, L.-z. Tang, P. Wang, X. Zhang, Microstructural evolution and mechanical behavior of friction spot welded 2198-T8 Al-Li alloy during aging treatment, Materials & Design, 115 (2017) 224-230.